JOURNAL OF SPACECRAFT AND ROCKETS
Vol. 32, No. 6, November–December 1995

Optimization of Hybrid-Rocket-Booster Fuel-Grain Design

D. J. Vonderwell,* I. F. Murray,† and S. D. Heister‡
Purdue University, West Lafayette, Indiana 47907

A ballistics model has been developed for investigating the influence of fuel-grain design on the overall performance of hybrid rocket boosters. The model, based on steady, one-dimensional compressible flow, includes the capability to handle arbitrary wagon-wheel fuel-section designs. To properly evaluate tradeoffs associated with a booster, stagnation-pressure losses are evaluated and a throttling capability is included. Results of the ballistics calculations are presented for both liquid oxygen and 90% hydrogen peroxide oxidizers assuming hydroxy-terminated polybutadiene as fuel. Vehicle interactions are considered by investigating a design capable of accomplishing the Titan 34D booster mission. Results indicate that the liquid-oxygen systems tend to optimize to a higher number of ports and mass-flux levels than the hydrogen peroxide systems.

Nomenclature

A = cross-sectional area, in.^{2}
A_t = throat area, in.^{2}
C_p = constant-pressure specific heat, Btu/lbm ·°R
C^* = characteristic velocity, ft/s
G_o = initial port oxidizer mass flux, lb/in.^{2}· s
G = total mass flux, lb/in.^{2}· s
H = stagnation enthalpy, Btu/lbm
L = fuel-grain length, in.
M = Mach number
$\mathcal{M}$ = molecular weight of chamber gases, lb/lb-mol
$\dot{m}_p$ = port oxidizer mass flow rate, lb/s
$\dot{m}_f$ = fuel mass flow rate, lb/s
OF = oxidizer/fuel ratio
P = pressure, psia
P_c = chamber (or stagnation) pressure, psia
Per = perimeter of fuel port
r_b = fuel regression rate, in./s
T = temperature, °R
T_c = chamber (or stagnation) temperature, °R
t = time, s
W = web distance, in.
x = axial distance from fuel-port entrance, in.
γ = Ratio of specific heats
ρ_f = fuel density, lb/in.^{3}

Introduction

RECENTLY, hybrid rockets have gained the attention of the rocket propulsion industry as a cost-effective means of providing boost propulsion for a variety of launch vehicles.[1–4] The hybrid system enjoys advantages over state-of-the-art solid propulsion systems in both specific impulse and throttlability. In addition, hybrid rockets are simpler to develop and operate than current bipropellant liquid systems, on account of the use of a single liquid.

One of the challenges in the design of a hybrid propulsion system involves the optimization of the fuel-section geometry (or grain design). Since both the exposed surface area and perimeter of fuel ports change with time, the mixture ratio will tend to shift during engine operation even if the oxidizer mass flow is held fixed. To achieve high volumetric efficiency within the combustion chamber, we desire high mass fluxes through the fuel ports. However, this desire is tempered by the fact that efficient combustion may not be possible at these high mass fluxes and that mixture-ratio shifts become more severe under these conditions. Even for a given mass flux, the number of fuel ports selected will have a significant effect in both thrust and specific-impulse histories for these propulsion systems.

Several authors[5–7] have identified the extent to which mixture-ratio shifts affect engine performance, but none of these sources have identified the overall interactions with booster design in these trade studies. In a significant effort, Ben-Yakar and Gany[7] developed a methodology to investigate hybrid-rocket ballistics for several different assumed fuel-port geometries. Their model assumed constant oxidizer flow rate and neglected stagnation-pressure losses along the length of the fuel port. We are also aware that various propulsion contractors have ballistics models with considerable sophistication,[8] although they have not been described in the open literature.

The capability of handling throttling of the oxidizer flow is crucial in booster applications, since throttling is desired near the point of maximum dynamic pressure during the ascent. In addition, it is desirable to be able to predict stagnation pressure losses within the fuel ports for a more accurate prediction of booster performance. Since both of these factors influence the stagnation pressure feeding the nozzle, they also influence the specific-impulse history.

To assess the contributions these issues have on propulsion-system design, we have developed a ballistics model capable of addressing variable oxidizer flow rate and fuel-section geometry. This model is described in the following section. The model has also been included in a hybrid-rocket preliminary sizing code[9,10] to assess interactions with the overall booster design. Results are presented assuming hydroxy-terminated polybutadiene (HTPB) as fuel for both liquid oxygen (LOX) and a 90% concentration of hydrogen peroxide (HP) as oxidizers.

Ballistics Model Development

A multiport wagon-wheel fuel-section design was selected for the model. A typical design (assuming eight ports) is shown in Fig. 1. A circular center port is also assumed (see Fig. 1) to minimize the amount of fuel slivers formed as the fuel is consumed. Fuel slivers are present between the center port and the wagon-wheel ports, as well as at the outer periphery of the grain. We assume that these slivers are not consumed during the firing, which leads to fuel-sliver predictions amounting to 2–4% of the total fuel volume for most cases investigated. These amounts are a bit smaller than those typically obtained in actual firings, but they are representative of the problem of consuming the entire fuel grain. The code is capable of handling wagon-wheel ports that are pie-shaped, i.e., with inner annulus of zero length.

Fuel-Grain Sizing

The flow down the ports was approximated as being one-dimensional, inviscid, and compressible. Complete mixing between the fuel and oxidizer at all points was also assumed at all stations

Received Aug. 2, 1994; revision received Nov. 1, 1994; accepted for publication Nov. 1, 1994.

*Graduate Student. Member AIAA.
†Undergraduate Student. Member AIAA.
‡Associate Professor, School of Aeronautics and Astronautics. Member AIAA.

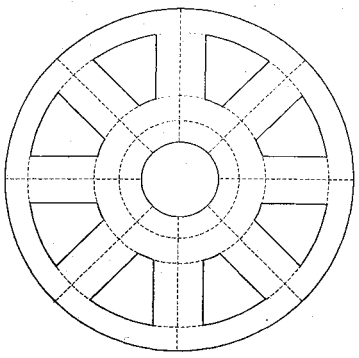

Fig. 1 Wagon-wheel fuel-grain cross section.

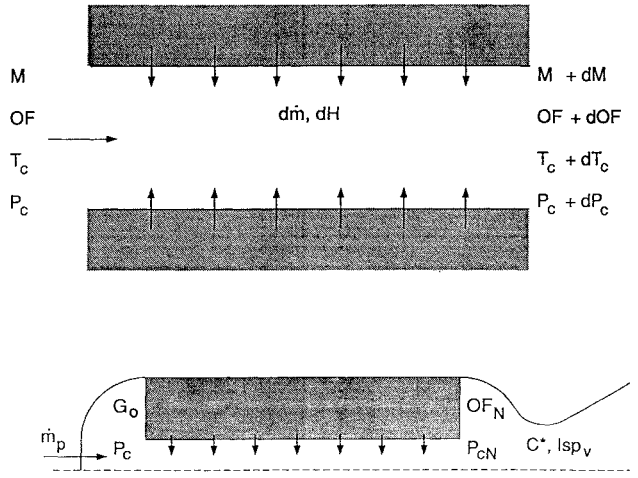

Fig. 2 Control volume for one-dimensional flow solution along a typical fuel port.

along the port. It was also assumed that the regression rate was constant along a port. Under these assumptions, the control volume at an arbitrary location x along the port is shown in Fig. 2. (See Nomenclature for definitions of variables.)

To initiate a port flow calculation, we presume that total burning time, the number of fuel ports, the total impulse requirement, the oxidizer massflux (G_o), and an average regression rate are known. The total usable mass of fuel and oxidizer is set by the impulse requirement and the desire to operate the engine at an optimal mixture ratio such that the specific impulse I_{sp} is maximized. Using the oxidizer mass from this requirement as well as the burning time, the total port area is calculated from $A_p = \dot{m}_p/G_o$. Using the assumed average regression rate and the burning time, we can also estimate the total fuel web thickness. The length of the ports is then determined by the fuel volume consistent with the impulse requirement.

Note that we take the initial cross-sectional area of the center port to be the same as those of the wagon wheels. We use this approach so that the initial regression rates will be the same in both of these regions. Further, we assume that the center port has the same regression rate as the outer ports for the duration of the firing even though its cross-sectional area history differs slightly from that of the wagon-wheel ports. This assumption is prudent, since only a small amount of the total burning surface is contributed by the center port in the multiport configurations that were considered in this study.

The fuel regression rate is assumed to behave as follows[8]:

$$r_b = 0.19G^{0.8}L^{-0.2} \tag{1}$$

where L is the length of the fuel grain and G is the total mass flux. While this regression model has been verified experimentally for the LOX–HTPB propellant combination, we will also assume that the HP–HTPB combination has identical behavior, because of the lack of data available for this oxidizer. Recent efforts[8,11] indicate that the exponent 0.8 on the mass-flux is correct for HP. Since Eq. (1) is an implicit expression (G is a function of r_b), we use a fixed-point iteration to determine the regression rate at a given time.

Port-Flow Solution

Since we are assuming a constant regression rate along the length of the port, then for a given port geometry the fuel flow rate is known at all points along the port:

$$\dot{m}_f = r_b \rho_f \text{ Per } x \tag{2}$$

where the variables are defined in the Nomenclature. Using this result, the local OF ratio is given by

$$\text{OF} = \dot{m}_p/\dot{m}_f \tag{3}$$

We assume complete mixing and local thermodynamic equilibrium, so that at a given pressure, the thermodynamic state of the mixture can easily be prescribed. To allow for the large variations in temperature, molecular weight, and specific heats, the parameters T_c, $\mathcal{M}$, C_p, and γ were all curve-fitted as a function of the local OF ratio by using the Gordon–McBride thermochemistry code,[12] assuming a chamber pressure of 1000 psi. These curve fits were demonstrated to be valid over a range of pressures from 400 to 1500 psi on account of the insensitivity of these parameters to the chamber pressure. The actual curve fits will not be included here in the interest of brevity.

The fluid entering a given port is assumed to be pure oxidizer. For LOX, we assumed the gases entered the ports at the saturation temperature of 162°R, while for HP we assumed the gases entered at the decomposition temperature of 1850°R. Radiative preheating and precombusting will surely raise the port inflow temperature in the case of LOX, but we had no simple means to quantify these effects in this study. In addition, we see a very rapid temperature rise in the entry region to the duct (see results section) such that reasonable gas temperatures are present at a very short distance into the length of the port without substantial pressure drop or Mach-number change. For these reasons, we feel that this assumption is adequate for the present study. The above assumption, in connection with the known port areas, allows us to compute the initial Mach number and static pressure of the oxidizer gasses entering the fuel port. These quantities serve as the initial conditions for the integration down the length of the port.

Using conservation of mass, momentum, and energy, Shapiro[13] relates changes in Mach number (M) and static pressure (P) to changes in total enthalpy (H), mass addition, and changes in properties. Frictional effects are neglected because of the low Mach number with the presence of wall blowing. The resulting differential equations relevant under these assumptions are

$$\frac{dM}{M} = F_1\left(\frac{dH}{C_pT} + \eta\frac{d\dot{m}}{\dot{m}} - \frac{d\mathcal{M}}{\mathcal{M}}\right) - \frac{1}{2}\frac{d\gamma}{\gamma} \tag{4}$$

$$\frac{dP}{P} = F_2\left(\frac{d\mathcal{M}}{\mathcal{M}} - \frac{dH}{H} - 2\eta\frac{d\dot{m}}{\dot{m}}\right) \tag{5}$$

where

$$\frac{dH}{C_pT} = \frac{d(C_pT_c) - (dC_p)\bar{T}}{C_pT} \tag{6}$$

$$F_1 = 0.5\frac{1+\gamma M^2}{1-M^2} \tag{7}$$

$$F_2 = \frac{\gamma M^2}{1-M^2} \tag{8}$$

and

$$\eta = 1 + \frac{\gamma - 1}{2}M^2 \tag{9}$$

Here, the quantity dH measures the change in stagnation enthalpy of a variable-property gas with $\bar{T}$ representing the average static

temperature over the interval of interest. Equations (4–9) are solved using a simple backward Euler numerical integration. All terms on the right-hand-side of Eqs. (4–6) are also differenced using a backward Euler procedure. Because of the low Mach numbers within typical hybrid-rocket-fuel ports, only 50–75 points were required to obtain accurate solutions to the equations.

At the end of the ports, the stagnation pressure loss due to the abrupt expansion is given by Kays[14]:

$$\Delta P_c = \frac{\gamma}{2} P_e M_e^2 \left(1 - \frac{A_p}{A_c}\right)^2 \tag{10}$$

where the subscript e refers to the port exit condition and the quantities A_p and A_c represent the total port and chamber cross-sectional areas.

Because the stagnation pressure down the length of the port is not known a priori, an iteration on the head-end chamber pressure is required. By integrating Eqs. (4) and (5) for an initial guess of the head-end pressure, we can obtain an estimate of the stagnation pressure feeding the nozzle (P_{cN}). We can also determine the stagnation pressure required to exhaust the calculated nozzle mass flow (simply the sum of all the port mass flows at the end of the ports) via

$$P_{\text{check}} = \frac{\dot{m}_N C^*}{A_t} \tag{11}$$

The characteristic velocity was curve-fitted as a function of the mixture ratio feeding the nozzle (OF_N) for both propellant combinations, assuming an aft-end pressure of 1000 psi. Results indicate that this curve fit is accurate for a considerable pressure range because of the insensitivity of C^* to this parameter.

In general, the calculated values of P_{check} will not agree with the P_{cN} value predicted by the port integration. The following iteration on the head-end stagnation pressure was employed to force convergence of these two pressures:

$$P_{c0}^{k+1} = P_{c0}^k + \frac{P_{\text{check}}^k - P_{cN}^k}{2} \tag{12}$$

where k is the iteration counter and P_{c0} is the head-end stagnation pressure. This iteration procedure converges to a pressure error of less than 0.1% in only a few iterations.

Following the convergence of the pressure iteration, the engine thrust and specific impulse can be determined. The theoretical vacuum I_{sp} was curve-fitted as a function of OF_N and the expansion ratio for each of the two propellant combinations, using Ref. 12 and assuming a pressure of 1000 psi. Results indicate that this curve fit is accurate over a substantial pressure range due to the insensitivity of the vacuum I_{sp} to this parameter.

At the end of the port-flow solution for a given web location, we increment the web distance and calculate the new time via

$$t^{k+1} = t^k + \Delta W / r_b^k \tag{13}$$

where ΔW is the selected web increment. Accurate results were obtained by using a web increment equal to 1/100 of the total web distance.

Model Validation

Convergence of the code has been demonstrated for the use of either constant or variable oxidizer flows for either of the two propellant combinations. In addition, the code was tested assuming constant-property, isothermal flow in which results can be compared directly with the analytic solution for one-dimensional (1-D) flow with mass addition. This comparison validated the port-flow algorithm. Finally, we have verified that the port-flow equations reduce to Rayleigh flow (1-D flow with heat addition) in the case of constant properties and zero mass addition.

An additional validation was employed by simulating the operation of the American Rocket Company 250,000-lbf thrust-motor test.[15] This motor employed a wagon-wheel grain design with 15 peripheral ports and a circular center port. The propellant combination used was LOX–HTPB. We had some difficulty in defining the exact geometry for this motor, since the details were not provided in Ref. 15. Using geometry scaled from Ref. 15, we obtained excellent agreement with the measured pressure drop of roughly 5% during early stages of the firing.

Ballistics-Model Results

The theoretical vacuum performance of the two propellant combinations is shown in Fig. 3. This figure indicates optimal mixture ratios of approximately 2.5 and 7.5 for the LOX and HP oxidizers, respectively. This figure also indicates that the LOX–HTPB combination is more sensitive to mixture-ratio shifts than the HP–HTPB combination. A typical port-flow solution for the temperature profile (nondimensionalized by the adiabatic flame temperature) is shown in Fig. 4 for two different G_o values. Note that the LOX–HTPB combination shows a rapid increase in temperature in the head-end portion of the port because of the low entry temperature discussed previously. Increasing mass flux has a rather minor effect on the temperature profile; it tends to push the stoichiometric point ($T = T_f$) upstream and decrease the port exit temperature, on account of the increased fuel regression and a shift to more fuel-rich operation.

Typical port stagnation-pressure loss characteristics are shown in Fig. 5. At the low oxidizer mass fluxes typical of state-of-the-art hybrid motors, the stagnation pressure losses are quite tolerable. While it is not apparent in this figure, the heat addition effect [dH/H term in Eq. (5)] is the dominant factor in determining the pressure loss. Mass-addition and variable-property effects are less significant, owing primarily to the low port entry Mach numbers (typically less than 0.01), consistent with the mass fluxes shown in Fig. 5. The LOX–HTPB combination exhibits higher losses than the HP–HTPB combination because there is a greater temperature change than with HP–HTPB. Losses due to mass addition are also

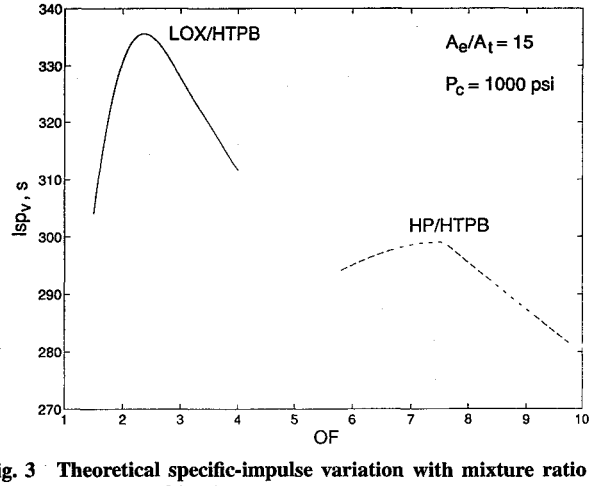

Fig. 3 Theoretical specific-impulse variation with mixture ratio for both propellant combinations.

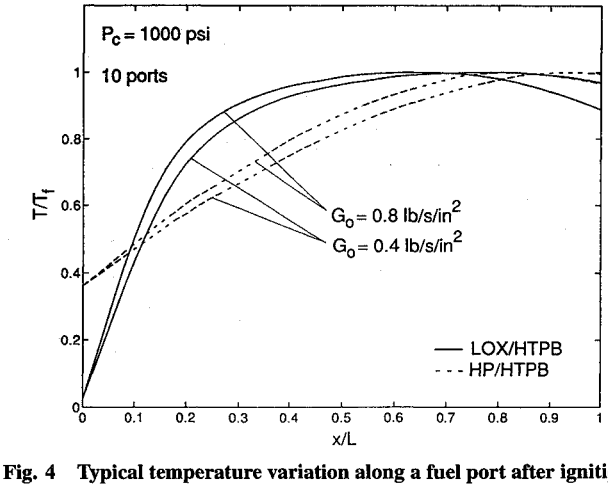

Fig. 4 Typical temperature variation along a fuel port after ignition.

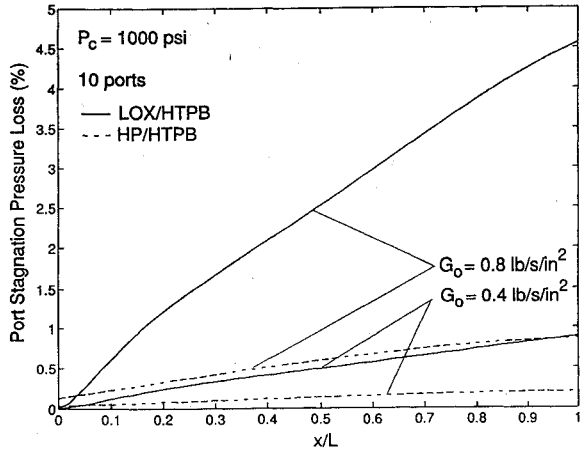

Fig. 5 Typical stagnation-pressure variation along a fuel port after ignition.

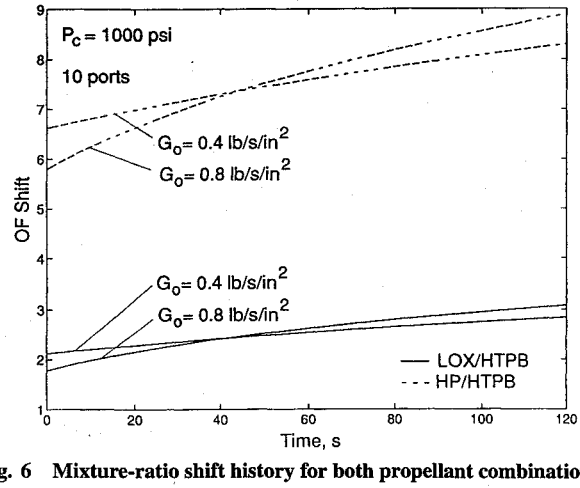

Fig. 6 Mixture-ratio shift history for both propellant combinations.

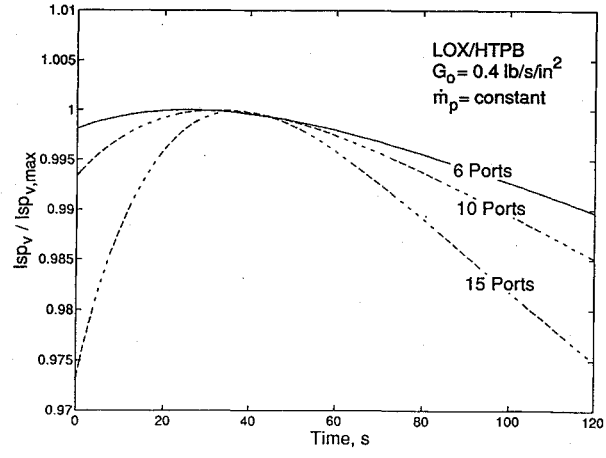

Fig. 7 Effect of port geometry on motor performance for LOX–HTPB propellant combination.

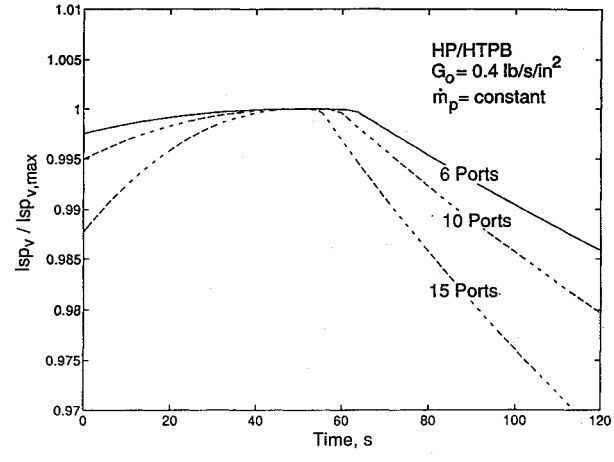

Fig. 8 Effect of port geometry on motor performance for HP–HTPB propellant combination.

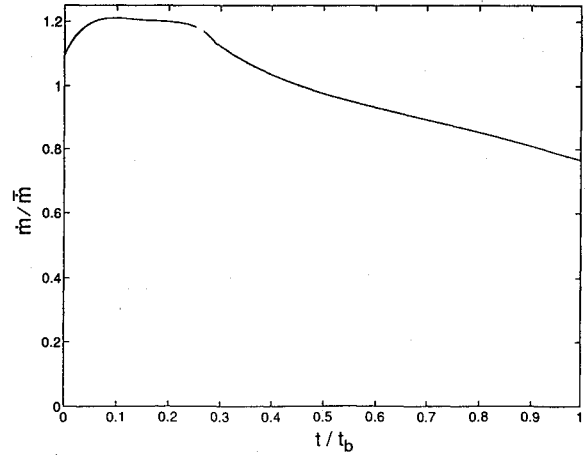

Fig. 9 Mass-flow history for Titan T34D solid rocket booster.

greater for LOX, because this oxidizer operates at lower mixture ratio than HP.

Figure 6 depicts mixture-ratio shifts for a typical 10-port configuration for both propellant combinations. The HP system exhibits a higher shift during operation, due to the sensitivity of the mixture ratio to small changes in fuel flow at high-mixture-ratio operation. Figures 7 and 8 highlight the effects of mixture-ratio shifts on vacuum I_{sp} for various port configurations for the LOX and HP oxidizers, respectively. Overall losses due to mixture-ratio shifts are in the 1–2% range for both oxidizers. Although the LOX–HTPB system is more sensitive to shifts in mixture ratio (Fig. 3), the overall shifts are smaller than for the HP–HTPB system. Combination of these two competing effects yields similar performance loss due to mixture-ratio variations. Increasing the number of ports tends to increase the percentage variation in port cross-sectional area (and hence regression rate), thus leading to a larger shift in mixture ratio. In comparing Figs. 7 and 8, it is apparent that the two oxidizers have comparable I_{sp} losses due to mixture-ratio shifts.

The effects of throttling have been addressed by utilizing a mass-flow history consistent with that of the Titan T34D solid rocket booster. The throttling history for this motor is shown in Fig. 9. High thrust is desired early in the flight when the vehicle is heaviest. A reduction in thrust about midway through the firing is desirable to reduce maximum dynamic pressure loads on the vehicle.

Using this mass-flow profile for the oxidizer, the effect on the vacuum I_{sp} is shown in Figs. 10 and 11 for the LOX and HP oxidizers, respectively. From these figures, it is apparent that throttling in the manner shown in Fig. 9 is actually beneficial to overall performance. In both cases, we note average I_{sp} losses less than 0.5% under throttled conditions. This behavior can be explained because the regression rate decreases with time as the ports burn out. Therefore, it is desirable to reduce oxidizer flow as well in order to remain near the optimal mixture ratio. For this reason, hybrid propulsion systems are particularly well suited to missions requiring regressive thrust histories (such as a strap-on booster).

Fuel-Section–Vehicle-Design Interactions

To assess the influence of fuel-section design on overall vehicle performance, the ballistics model discussed above has been incorporated in a hybrid-booster preliminary sizing code.[9,10] The booster is designed to accomplish a mission equivalent to that of the $5\frac{1}{2}$-segment booster utilized on the Titan 34D launch vehicle.[16] All designs were based on a 2-min burning time and an equivalent

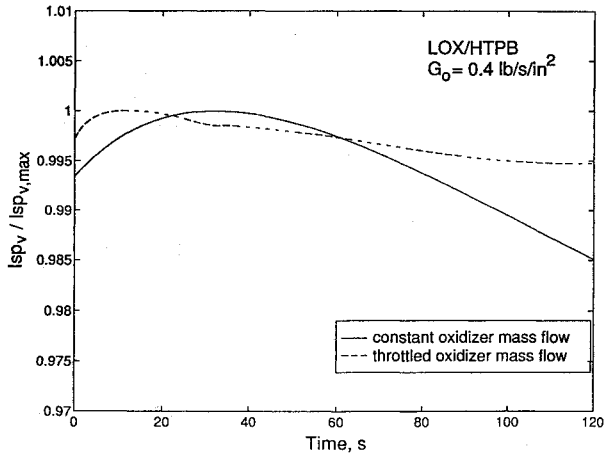

Fig. 10 Effect of throttling on motor performance for LOX–HTPB propellant combination.

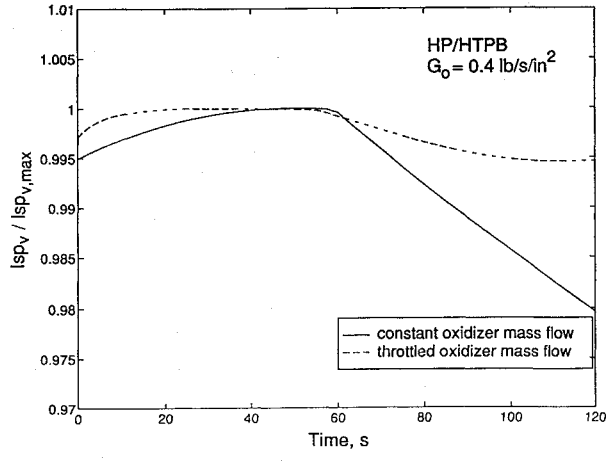

Fig. 11 Effect of throttling on motor performance for HP–HTPB propellant combination.

constant ambient pressure corresponding to an altitude of 50,000 ft. The throttled-oxidizer-flow history shown in Fig. 9 was used for all simulations. Unfortunately, changes in vehicle drag associated with different booster designs have not been considered in the present results.

Figure 12 depicts the sensitivity of the booster gross liftoff weight to changes in port mass flux for both propellant combinations. As the mass flux is increased, the fuel-section size is decreased, but the mixture-ratio shifts become larger, causing reductions in specific impulse. Results indicate that the effect of the mixture-ratio shift is dominant for the HP–HTPB propellant, but fuel-section size is dominant for the LOX–HTPB propellant. This interesting result is attributed to the fact that the LOX fuel section is much larger and represents a larger fraction of the total mass than the HP. We should note that we saw similar behavior for LOX at larger numbers of fuel ports. We remind the reader that aerodynamic drag effects have not been considered in these results. That factor may not change the conclusions substantially, since all designs had diameters that were within a ±10% range.

Figure 13 presents the optimization of the number of ports for both propellant combinations at fixed G_o and chamber pressure. In this figure, all boosters were sized to attain the same velocity increment, consistent with that of the Titan 34D vehicle.[16] Increases in gross liftoff weight (above the minimum levels shown in the figure) are attributed to I_{sp} losses associated with mixture-ratio shifts as well as changes in booster inert weights. The results in Fig. 13 indicate that the HP–HTPB system optimizes at 10 ports, whereas the lower-mixture-ratio LOX–HTPB system shows a broad trough in the 15–20-port range. For the LOX–HTPB system, increasing G_o tended to decrease the optimal number of ports; but this was at the expense of an increase in vehicle weight, as indicated in Fig. 12. For a large

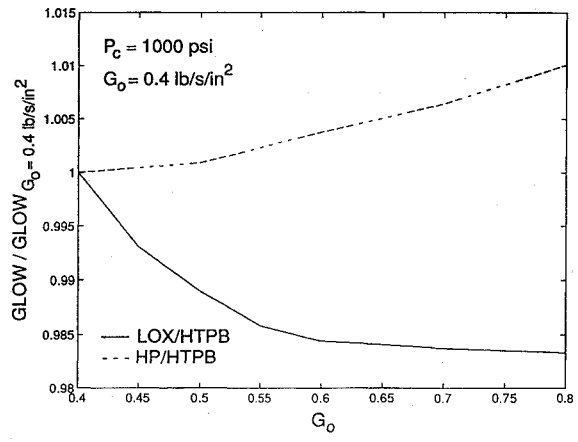

Fig. 12 Sensitivity of booster gross liftoff weight to changes in initial port mass flux.

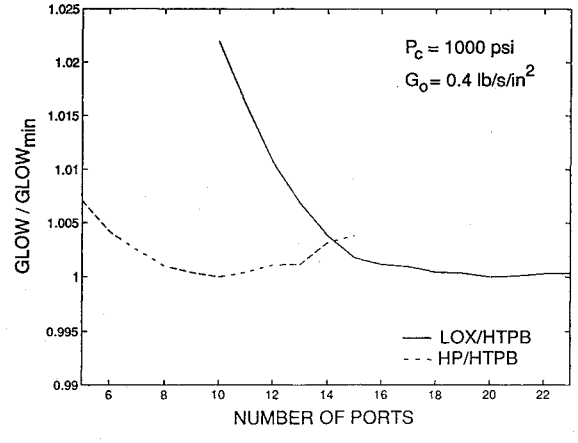

Fig. 13 Sensitivity of booster gross liftoff weight to the number of fuel ports.

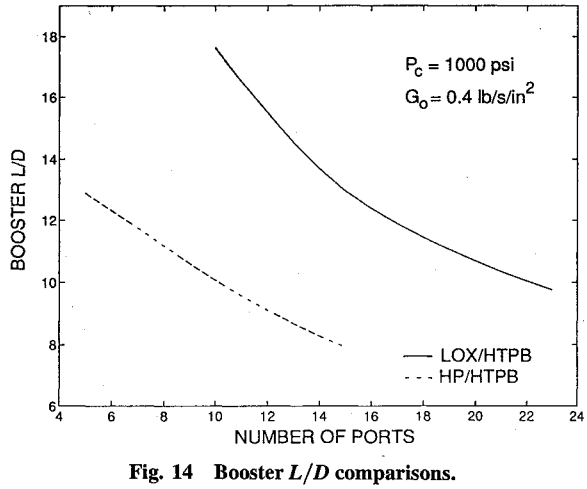

Fig. 14 Booster L/D comparisons.

number of ports, we did experience some difficulties in the I_{sp} curve fit going out of range on the fuel-rich side during the early part of the firing. The nonphysical wiggles in the curves are attributed to this minor effect.

The resulting booster lengths (for the conditions noted) are presented in Fig. 14. Increasing the number of ports has the obvious effect of decreasing the length in general. The HP–HTPB boosters are shorter because of the higher propellant bulk density and more compact fuel section associated with the higher optimal mixture ratio. For the LOX–HTPB system, booster diameters varied over the range of 102–123 in. between the 10- and 23-port cases, respectively. For the HP–HTPB system, booster diameters varied between 110 in. for the 5-port configuration and 127 in. for the 15-port configuration.

Conclusions

A ballistics model has been developed to assess the influence of fuel-section design on the performance of hybrid rocket boosters. The model has the capability to predict stagnation-pressure losses along the fuel ports, and can handle an arbitrary time-dependent (throttled) oxidizer flow. Results indicate that though the LOX–HTPB system is more sensitive to mixture-ratio shifts than the HP–HTPB, the overall performance loss is comparable for the two systems, since HP–HTPB experiences a greater shift during operation. Throttling the oxidizer flow using the Titan 34D mass-flow profile yields an improvement in performance over the constant-flow case. This improvement is attributed to the fact that mixture-ratio shifts are diminished with the variable oxidizer flow.

Vehicle interactions have been considered for a booster designed to accomplish a mission equivalent to the Titan 34D solid motor. The booster gross liftoff weight increases with increasing oxidizer mass flux for the HP–HTPB propellant, whereas the LOX–HTPB propellant exhibits an opposite trend. The HP–HTPB system optimizes at 10 wagon-wheel ports for the configuration studied, whereas the LOX–HTPB system showed a broad minimum in the 15–20-port range.

Acknowledgment

The authors would like to acknowledge the contributions of John Brown in providing programming support for the hybrid-rocket sizing code described in this study.

References

[1]Kniffen, R. G., McKinney, B., and Estey, P., "Hybrid Rocket Development at the American Rocket Company," AIAA Paper 90-2762, July 1990.

[2]Whittinghill, G. R., and McKinney, B. C., "The Aquila Launch Service for Small Satellites," AIAA Paper 92-3588, July 1992.

[3]Atlantic Research Corp., "Hybrid Propulsion Technology Program," Final Rept., Atlantic Research Corp., NASA-CR-183952, Gainesville, VA, Jan. 1990.

[4]Altman, D., "Hybrid Rocket Development History," AIAA Paper 91-2515, June 1991.

[5]Waidmann, W., "Thrust Modulation in Hybrid Rocket Engines," *Journal of Propulsion and Power*, Vol. 4, No. 5, 1988, pp. 421–426.

[6]Osman, R. V., "An Experimental Investigation of a Lithium Aluminum Hydride–Hydrogen Peroxide Hybrid Rocket," *Aerospace Chemical Engineering, Chemical Engineering Progress Symposium Series*, Vol. 62, No. 61, 1965, pp. 92–102.

[7]Ben-Yakar, A., and Gany, A., "Hybrid Engine Design and Analysis," AIAA Paper 93-2548, June 1993.

[8]McFarlane, S., private communication, American Rocket Co., Ventura, CA, Feb. 1994.

[9]Werthman, W. L., and Schroeder, C. A., "A Preliminary Design Code for Hybrid Propellant Rockets," AIAA Paper 94-0006, Jan. 1994.

[10]Ventura, M., and Heister, S., "Hydrogen Peroxide as an Alternate Oxidizer for a Hybrid Rocket Strap-on Booster," AIAA Paper 93-2411, June 1993.

[11]Wernimont, E., and Meyer, S., "Hydrogen Peroxide Hybrid Rocket Engine Performance Investigation," AIAA Paper 94-3147, June 1994.

[12]Gordon, S., and McBride, B. J., "Computer Program for Calculation of Complex Chemical Equilibrium Compositions, Rocket Performance, Incident and Reflected Shocks, and Chapman-Jouguet Detonations," NASA SP-273, June 1971.

[13]Shapiro, A. H., *The Dynamics and Thermodynamics of Compressible Flow*, 1st ed., Vol. 1, Ronald Press, New York, 1953, pp. 220–227.

[14]Kays, W. M., "Loss Coefficients for Abrupt Changes in Flow Cross Section with Low Reynolds Number Flow in Single and Multiple Tube Systems," *Transactions of the American Society of Mechanical Engineers*, Paper 50-S-7, Vol. 72, July 1950, pp. 1067–1074.

[15]McFarlane, J. S., and Lichatowich, J., "Design and Testing of AMROC's 250,000 lbf Thrust Hybrid Motor," AIAA Paper 93-2551, June 1993.

[16]Heister, S. D., "Propellants for Low Cost Solid Rocket Boosters," The Aerospace Corp., TOR-0086(6453-01)-1, El Segundo, CA, Feb. 1986.

J. A. Martin
Associate Editor